6.1 Introduction

After all of this discussion of the production of radiation at accelerators, it is now advisable to discuss in one place the relevant properties of the most common materials used in radiation shielding. Such a discussion will be presented in this chapter. Since many shielding problems are driven by the nature of the energy spectrum of the neutrons, such spectra are also discussed here in some detail and examples of neutron energy spectra measured external to shielding at various types of accelerator facilities are presented.

6.2 Discussion of Shielding Materials Commonly Used at Accelerators

Given the size of many modern accelerators, economic considerations typically dominate shielding designs by requiring the use of relatively inexpensive, but less efficient shields. Aside from the need to accomplish the identified goals in radiation safety, in all situations good engineering practices concerning structural properties, appropriate floor loading allowances, and fire protection must be taken into account to provide an acceptable level of occupational safety. In general, low atomic number materials are best used for targets, collimators, and beam stops at electron accelerators to reduce photon production, while high atomic number materials are preferred at proton and heavy ion accelerators for these components to reduce neutron production. From the previous chapters, it should be clear that at energies above 5 MeV neutrons are produced in most materials. Some materials have superior heat transfer characteristics that enhance reliability and thus can reduce personnel exposures incurred in maintenance activities.

6.2.1 Earth

Earth has many admirable qualities as a shield material besides its low cost. Especially important is that the water it contains enhances the effectiveness of the neutron attenuation. This is because the mass of a proton is essentially equal to that of a neutron. As a result of conservation of energy and momentum conservation, in an elastic collision, the energy that can be transferred from a neutron having kinetic energy E_o to a target nucleus, ΔE, as a function of scattering angle θ, is given by

$$\frac{\Delta E}{E_o} = \frac{4\frac{M}{m_n}\cos^2\theta}{\left(1+\frac{M}{m_n}\right)^2}, \qquad (6.1)$$

where M is the mass of the recoiling nucleus and m_n is the mass of the incident neutron. Thus, at small scattering angles (i.e., $\theta \approx 0$), nearly all of the neutron kinetic energy can be transferred to the protons in the water. On the other hand, ^{12}C nuclei are capable of

absorbing only 28 per cent of the incident neutron energy. The proton energy, then, can be dissipated in the medium by means of ionization and other nuclear interactions. Representative ranges of soil water content (per cent of dry weight) are: sand (0-10), sandy loam (5-20), loam (8-25), silty loam (10-30), dry loam (14-30), and clay (15-30).

Additionally, earth is also composed of sufficiently high atomic number elements to be effective against photons. Dry earth has a typical elemental composition as given in Table 6.1 due to Chilton (Ch84). Earth is generally a "crackless" shield, not prone to neutron leakage by "streaming". The density of earth varies widely, from as low as 1.7 g cm^{-3} to as much as 2.25 g cm^{-3} , depending upon soil type and water content. In general, sandy soils will have lower values of density than heavy clays found in glacial till. Extrusive volcanic soils, on the other hand, can have very low densities. Given this variation, specific knowledge of soil characteristics at the accelerator site are needed to do effective shielding designs. Definitive measurements of the water content are also most useful if the shielding of neutrons is the intent and no safety factors are being used.

Table 6.1 Elemental composition, dry-weight percent, of representative soils. [Adapted from (Ch84).]

Element	Global Average (%)
O	43.77
Si	28.1
Al	8.24
Fe	5.09
Mn	0.07 ± 0.06
Ti	0.45 ± 0.43
Ca	3.65
Mg	2.11
K	2.64
Na	2.84

6.2.2 Concrete

Concrete has obvious advantages in that it can either be poured in place permanently or be cast into modular blocks. Sometimes concrete is used to shield targets, beam stops, etc. in a manner that allows their ready access if the need for maintenance arises. The use of concrete blocks generally requires the overlapping of the blocks to avoid **streaming** through the cracks. It is sometimes efficient to use a heavy material as part of the aggregate in the concrete recipe. This can increase the density of the material as well as its average atomic number. The latter, of course, increases the effectiveness against photons. Table 6.2 due to Chilton (Ch84) gives some partial densities of various concretes used in shielding, thus illustrating the elemental variability found in the composition. When shielding neutrons, the water content is quite important because it incorporates almost all of the hydrogen. Under extreme low-humidity conditions, the

water content of concrete can decrease with time, to as little as 50 % of the initial value over a 20 year period. The density of concrete is locally variable.

Table 6.2 Partial densities of representative concretes after curing. [Adapted from (Ch84).]

Type:	**Ordinary**	**Magnetite**	**Barytes**	**Magnetite & Fe**
Additive		**(FeO, Fe_2O_3)**	**$BaSO_4$**	
Density (g cm^{-3}):	**2.34**	**3.53**	**3.35**	**4.64**
H	0.013	0.011	0.012	0.011
O	1.165	1.168	1.043	0.638
Si	0.737	0.091	0.035	0.073
Ca	0.194	0.251	0.168	0.258
Na	0.040			
Mg	0.006	0.033	0.004	0.017
Al	0.107	0.083	0.014	0.048
S	0.003	0.005	0.361	
K	0.045		0.159	
Fe	0.029	1.676		3.512
Ti		0.192		0.074
Cr		0.006		
Mn		0.007		
V		0.011		0.003
Ba			1.551	

6.2.3 Other Hydrogenous Materials

6.2.3.1 Polyethylene and other Materials That Can Be Borated

Polyethylene, $(CH_2)_n$, is a very effective neutron shield because of its hydrogen content (14% by weight) and its density ($\approx$ 0.92 g cm^{-3}). It can thus attenuate so-called "fast" neutrons. In many circumstances, it provides very adequate shielding and is highly efficient due to the high hydrogen content. Thermal neutrons can be captured through the $^1H(n,\gamma)^2H$ reaction which has a cross section of 0.33 barn for neutrons in thermal equilibrium at room temperature (E_n = 0.027 eV). The emitted γ-ray has an energy of 2.2 MeV that provides a somewhat troublesome source of radiation exposure in some situations. The addition of boron can reduce the buildup of 2.2 MeV photons released in the thermal neutron capture by hydrogen by instead capturing the thermal neutrons in the boron, by means of the $^{10}B(n,\alpha)^7Li$ reaction. The latter has a cross section for "room temperature" neutrons of 3837 barns. In 94 per cent of these captures, the emitted α-particle is accompanied by a 0.48 MeV γ-ray. The α-particle is readily absorbed by ionization while the γ-ray has a much shorter attenuation length than does a 2.2 MeV γ-ray. Commercially, polyethylene is available that includes additives of boron (up to 32%), lithium (up to 10 %) and lead (up to 80 %) in various forms such as planer sheets, spheres, and cylinders.

These materials can be useful, if it is necessary, to economize on space and also to accomplish shielding of photons and neutrons simultaneously. Pure polyethylene is flammable, but some of the commercial products available contain self-extinguishing additives. Some of these materials are available in powder form, for molding into a desired shape by the user. Besides polyethylene, boron has been added to other materials to form effective thermal neutron shields. These include other plastics, putties, clays, and glasses to accomplish specific shielding objectives. Plastic materials such as polyethylene can also be subject to significant radiation damage at relative low levels of integrated absorbed dose (Sc90). The effects upon the structural integrity must be carefully considered in such circumstances.

6.2.3.2 Water, Wood, and Paraffin

These materials are superficially attractive neutron shields because of their very high hydrogen contents.

Water, of course, tends to rust out its containers and there is the omnipresent question as to whether the shield material has flowed away. Exposed to thermal neutrons, it also emits the 2.2 MeV capture γ-ray from hydrogen. The addition of boron is more difficult because of the relative insolubility of boron salts in water. However, potassium tetraborate is relatively soluble in water.

Wood was found in the early years of operation at the Bevatron at the Lawrence Radiation Laboratory (now the Lawrence Berkeley National Labortory) to be as effective per unit length as concrete for shielding intermediate energy neutrons. Thus, it is essential that the neutron energy spectrum to be attenuated is known. In the past wood has been discouraged as a shielding material because of its flammability. Recently, chemically treated wood that is nearly completely fireproof has become available, but it is not clear that the flammability problem has been solved with complete satisfaction. Also, questions have been raised by reports of a reduction in structural strength of such treated wood products.

Paraffin historically has been used for neutron shielding but has been spurned because of the fire hazard. Under some conditions it can be used if it is packaged in metal containers. Recently, paraffin treated with fire retardant additives has become available. This material is subject to "plastic" flow problems.

6.2.4 Iron

A relatively high density, in conjunction with its low cost, makes iron an attractive shielding material. Caution is required because the density can vary widely from a low of 7.0 for low-grade cast iron to a high value of 7.8 g cm^{-3} for some steels. The "textbook" value of 7.87 g cm^{-3} given in Table 1.2 is almost never attained in the bulk quantities necessary for radiation shielding. Because of its nonmagnetic properties and resistance to corrosion, stainless steel is often used as part of accelerator components. Because of

concerns about radioactivation (see Chapter 7), knowledge of the elemental composition of various alloys can sometimes be of interest. For example, long-lived ^{60}Co can be produced in stainless steel but not in pure iron. While tempting, the use of steel wool to fill cracks in a large shield is undesirable due to the contamination hazard presented by the resulting rust. Iron has a very important deficiency as a neutron shield; this will be discussed in Section 6.3.5.

6.2.5 High Atomic Number Materials (Lead, Tungsten, and Uranium)

The materials in this category are valuable because of their high atomic number, especially where the shielding of photons is important. The most obvious material in this category is *lead*. It has high density (11.3 g cm^{-3}) and is resistant to corrosion. Pure lead, as is well known, has major drawbacks because of its poor structural characteristics and low melting point (327.4 ^{o}C). It is usually best used when it can be laminated to some other, more structurally stable, material. Some alloys represent improvements on the structural properties. It is often available as an additive to other materials in order to improve their capacity for shielding photons. Fabric blankets containing shredded lead can be effectively used to shield radioactivated components to minimize exposures associated with accelerator maintenance activities during operational shutdowns. The high chemical toxicity of lead requires care in its fabrication and handling to properly protect personnel. The use of lead wool to fill cracks is discouraged due to the chemical toxicity hazard. Bismuth, having a density of 9.7 g cm^{-3}, is sometimes used as a lower-toxicity substitute for shielding against photons.

Tungsten is an excellent, but relatively expensive, shielding material. Its high density (19.3 g·cm^{-3}) and high melting temperature (3410 ^{o}C) make it extremely useful as a component in photon shields and in beam collimators. It is difficult to machine, so alloys such as Hevimet are commonly used. Hevimet was developed by the General Electric Co. It consists of tungsten (90%), nickel (7.5%) and copper (2.5%), and has a typical density 16.9 to 17.2 g cm^{-3} (Ma68). It is currently commercially available from several sources and in various forms exemplified by HD18[1]. HD18 is 95% tungsten, 3.5% nickel, and 1.5% copper, and has a density of 18 g cm^{-3}.

Uranium is a superficially attractive shielding material, most often in its "depleted" form in which ^{235}U is removed from the naturally dominant ^{238}U down to some residual fraction (usually 0.2 %) much lower than the natural value of 0.72 %. Its high density (19.0 g·cm^{-3}) and relatively high melting point (1133 ^{o}C) are positive attributes, especially in places where space efficiency is a concern. It is obviously not a good choice of material in environments having a high neutron flux density due to its susceptibility to fission induced by fast neutrons. In the depleted form, it is relatively safe, but if combined with hydrogenous materials, nuclear fission criticality should be considered for the specific material and geometric arrangement to be employed. Even in the absence of hydrogen, thermal neutrons under certain conditions can result in the possibility of

[1] Mi-Tech Metals, Inc., 1340 N. Senate Ave., Indianapolis, Indiana 46202

criticality if insufficiently depleted of ^{235}U (Bo87). Major drawbacks are its material properties. It has a large anisotropic thermal expansion coefficient and also readily oxidizes when exposed to air (especially humid air). The oxide is readily removable and presents a significant internal exposure hazard. Prevention of oxidation by sealing it with epoxy or paint meets with only limited success due eventual embrittlement and chipping accelerated by radiation damage. Sealed containers filled with dry air or with noble gases or liquefied noble gases such as argon seem to represent the best storage solution to limit oxide formation. Small chips of this element are also pyrophoric, complicating machining-type processes by posing yet another safety hazard. Uranium in any form, as a "nuclear material", is subject to stringent accountability requirements.

6.2.6 Miscellaneous Materials (Beryllium, Aluminum, and Zirconium)

These three materials find considerable usage as accelerator components because of various properties. *Beryllium* is often used as a target material in intense beams because of its resistance to thermal effects, especially when in the form of the oxide, BeO. It has been used at high energy accelerators in relatively large quantities as a "filter" to enrich one particle type at the expense of another. A serious concern is the extreme chemical toxicity of the metal and its compounds, which makes it difficult to fabricate. *Aluminum* is used in accelerator components because of its nonmagnetic properties and its resistance to corrosion. It is not an effective shield against neutrons. *Zirconium* has a very small thermal neutron capture cross section and very good thermal properties. It is therefore not a good neutron absorber but has been found to be useful in beam-handling component material in some situations.

6.3 Neutron Energy Spectra Outside of Shields

As has been discussed in the previous chapters, at most accelerators, except perhaps for forward shielding at high energy accelerators capable of producing muons, the shielding is largely designed largely to attenuate neutrons. In this section, examples of neutron energy spectra commonly found at accelerators external to shielding are presented and discussed. While individual spectra may vary a great deal from these examples, which are not intended to be comprehensive, the general principles are of interest.

6.3.1 General Considerations

In the most simple approximation, outside of thick shields of soil or concrete that contain some hydrogen content (usually in the form of H_2O), accelerator neutron shields can most generally said to be to zeroth order proportional to inverse energy. Such "*1/E*" spectra can have energies extending from those of thermal neutrons ($<E_n>$ = 0.025 eV) up to the energy of the incident particles, but are commonly effectively cut off at some upper energy that is less then the incident particle energy. Thus, at this level of approximation, the spectrum is given as:

$$\frac{d\phi(E)}{dE} = k\frac{1}{E}, \tag{6.2}$$

where k is a normalizing constant. Rohrig (Ro83) observed from this that it often is more convenient to plot such spectra as flux per *logarithmic* energy interval by simply plotting $E\phi(E)$;

$$\frac{d\phi(E)}{d\ln E} = E\phi(E)\ . \tag{6.3}$$

In the terminology of textbooks on neutron physics, this is also called a "lethargy" plot. It, effectively, suppresses the 1/E dependence seen in typical neutron energy spectra. Most, but not all, of the example spectra discussed further are presented as lethargy plots.

6.3.2 Examples of Neutron Spectra Due to Incident Electrons

Alsmiller and Barish have performed calculations of the neutron energy spectra that arise when 400 MeV electrons are incident on a thick copper target (Al73). These calculations also predicted the neutrino yields over several ranges of production. They considered four different shielding materials; soil, concrete, ilmenite ($FeTiO_3$), and iron. Calculations of neutron energy spectra and the fractional contributions to the total dose equivalent from neutrons with energies less than a given energy E for the same spectrum for the angular region $0 < \theta < 30^o$ are presented in Fig. 6.1. These results are for a radial depth in the shield of 7 mean free paths of the highest energy neutrons found in this source spectrum within this angular range. Table 6.3 gives the densities and the neutron mean free paths used for the four materials.

Table 6.3 Material properties used in the calculations of Alsmiller and Barish [Adapted from (Al73).]

Material	Density ($g\ cm^{-3}$)	Mean Free Path ($g\ cm^{-2}$)
soil	1.8	103.6
concrete	2.3	105.3
ilmenite	3.8	120.6
iron	7.8	138.6

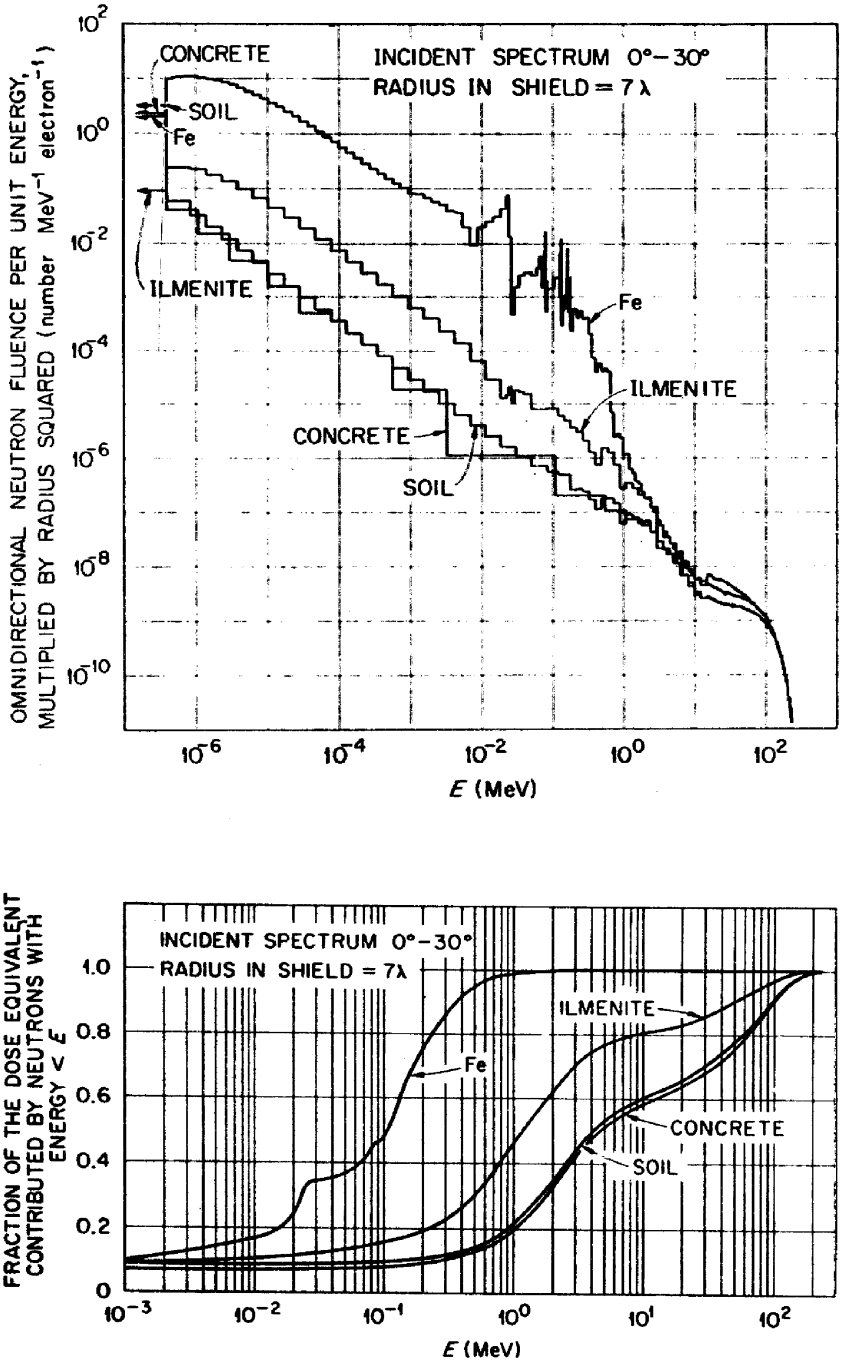

Fig. 6.1 Neutron spectral information from 400 MeV electrons incident on a thick Cu target. The **upper frame** shows the omnidirectional neutron fluence per unit energy multiplied by the square of the radial depth in the shield as a function of energy for the various shield materials studied by Alsmiller and Barish. The **lower frame** shows the fractional contribution to the total dose equivalent from neutrons with energies less than E as a function of E for shielding materials. [Reproduced from (Al73).]

In this figure, the inverse square dependence was removed to remove "geometrical" attenuation within the shield. It should be clear that the neutron spectra in the iron shield is markedly different from that found in the soil and concrete shields. The characteristics of the spectra found in the ilmenite are intermediate, perhaps related to the presence of iron in this material. The same kinds of phenomena associated with iron shielding are found in neutron energy spectra measured at high energy proton accelerators. Special considerations pertaining to iron spectra will be discussed in Section 6.3.5.

6.3.3 Examples of Neutron Spectra Due to Low and Intermediate Energy Protons

Calculations and measurements of neutron energy spectra at various depths in shielding due to 52 MeV protons have been reported by Uwamino et al. (Uw82). These results are presented in Fig. 6.2.

Alsmiller, et al. (Al75) has provided predictions of neutron energy spectra averaged over specific angular intervals for 200 MeV protons stopped in a thick water target. The results are given for large angles are presented in Fig. 6.3.

6.3.4 Examples of Neutron Spectra Due to High Energy Protons

In the regime of proton energies well above one GeV, the details of the spectra are far more sensitive to geometrical considerations than they are dependent upon the incident proton energy. O'Brien carried out a calculation of a generalized neutron spectrum that could be found external to a high energy accelerator (OB71). These were compared with measurements and alternative calculations performed by Höfert and Stevenson (Hö84a). The results are provided in Fig. 6.4 for both "lateral" and "forward" angular regions. The results for forward angles also include the spectra of charged pions and protons. It is clear that at the forward angles, the total fluence of hadrons at high energies is likely to be a mixture of charged particles and neutrons.

Detailed features of the geometry involved can produce peaks in the neutron energy spectrum. Examples of such spectra have been provided by various workers (Pa73, Th88, El86, McC88, and Co88). These peaks are typically encountered in the few MeV region. Figures 6.5, 6.6, 6.7, and 6.8 are plots of neutron spectra and sketches of the shielding geometry involved taken from Cossairt et al. (Co88). These spectra were obtained (i.e., "unfolded") using the Bonner sphere technique discussed in more detail in Chapter 9. In these four figures, “spheres” denote the locations where the neutron energy spectra were measured. These are typical of the spectra found at high energy proton accelerators. Figure 6.5 is rather typical of the spectra found external to earth and concrete shields lateral to high energy proton accelerators. The neutron energy spectrum displayed in Fig. 6.6 is particular interesting because its shape was demonstrated to be essentially independent of proton energy over the range of 150 to 900 GeV (McC88). Fig. 6.7 is typical of the results obtained in the second and succeeding sections (“legs”) of a labyrinth penetration.

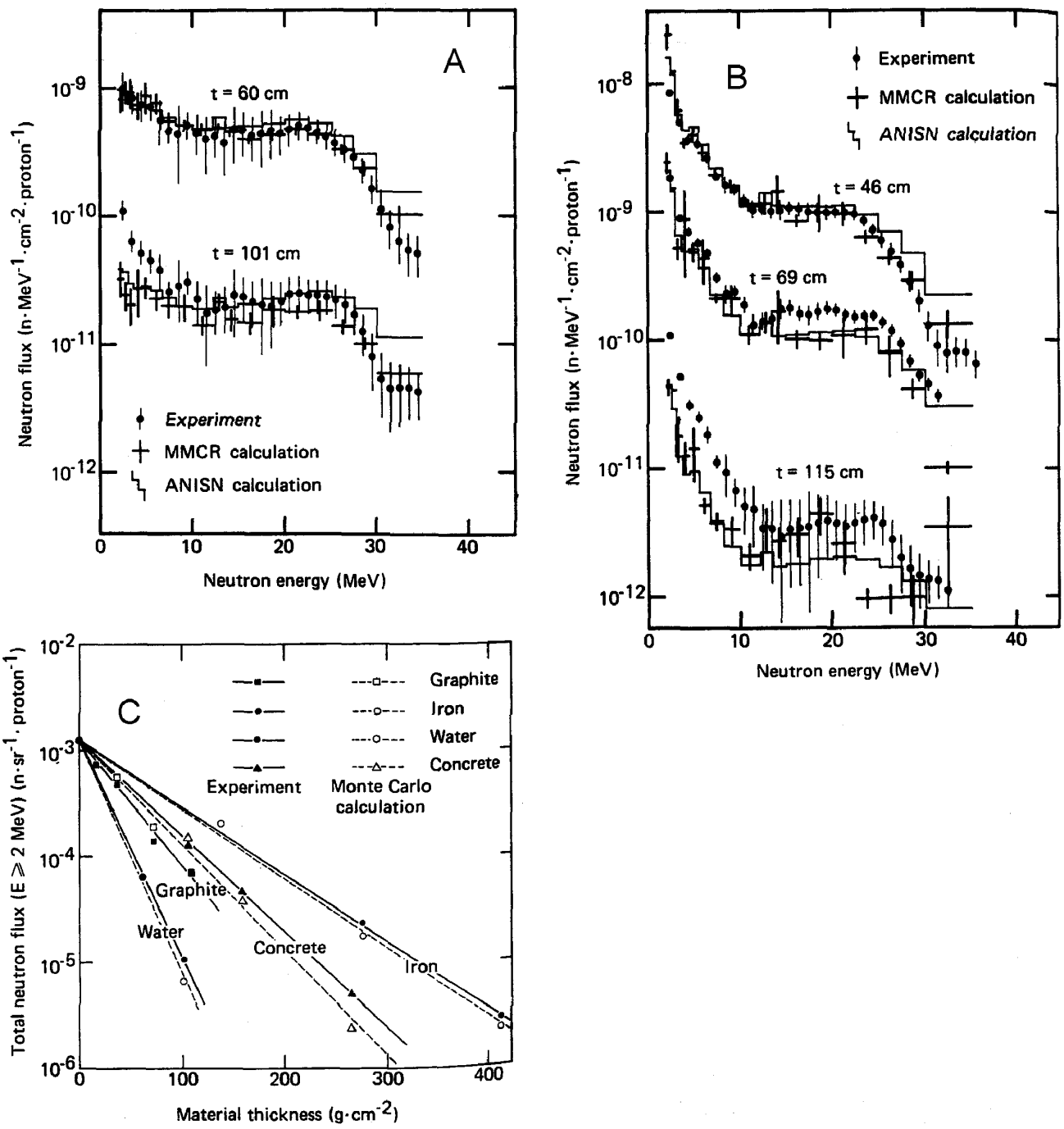

Fig. 6.2 Forward neutron energy spectra and attenuations measured and calculated by Uwamino et al. for 52 MeV protons. The protons interacted with the material being studied. Following a distance, *t*, the spectra were determined at θ = 0. Frame **A** displays spectra for water at two different values of *t*, frame **B** displays spectra for ordinary concrete at two different values of *t*, and frame **C** provides data on the attenuation profiles for various materials. [Adapted from (Uw82).]

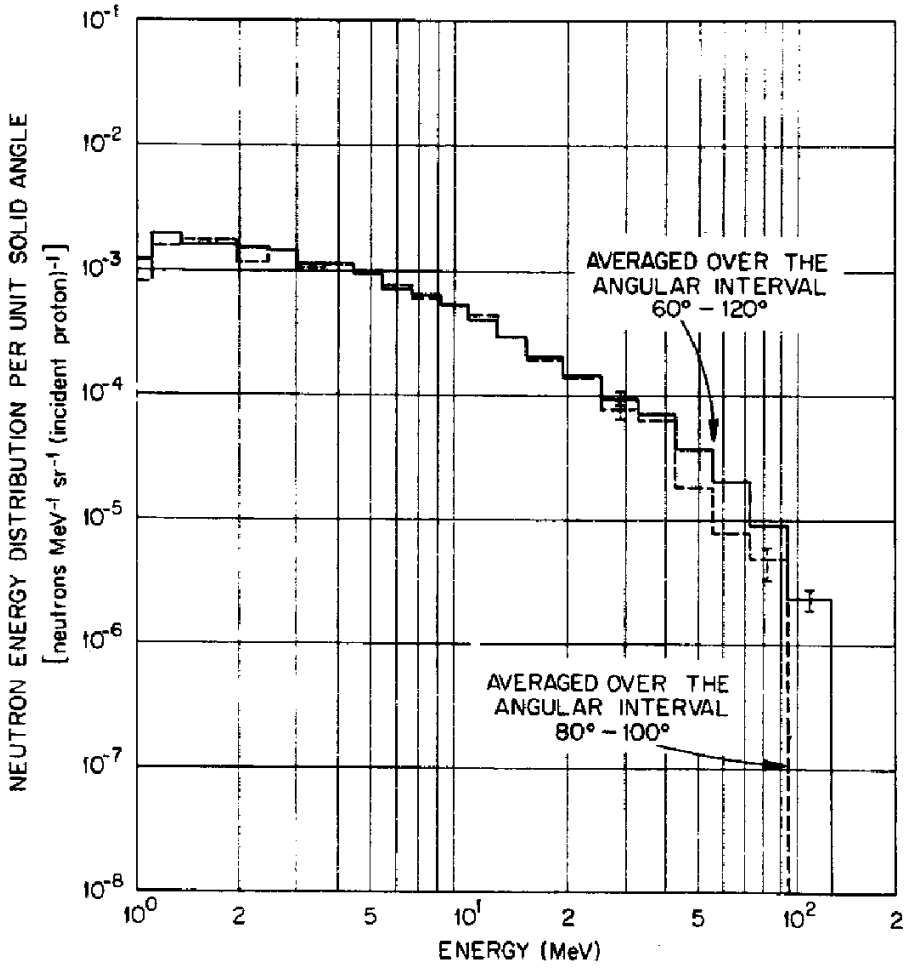

Fig. 6.3 Energy distribution of neutrons averaged over particular angular intervals, produced when 200 MeV protons are stopped in a thick water target. The protons are incident at $\theta = 0^{o}$. [Adapted from (Al75).]

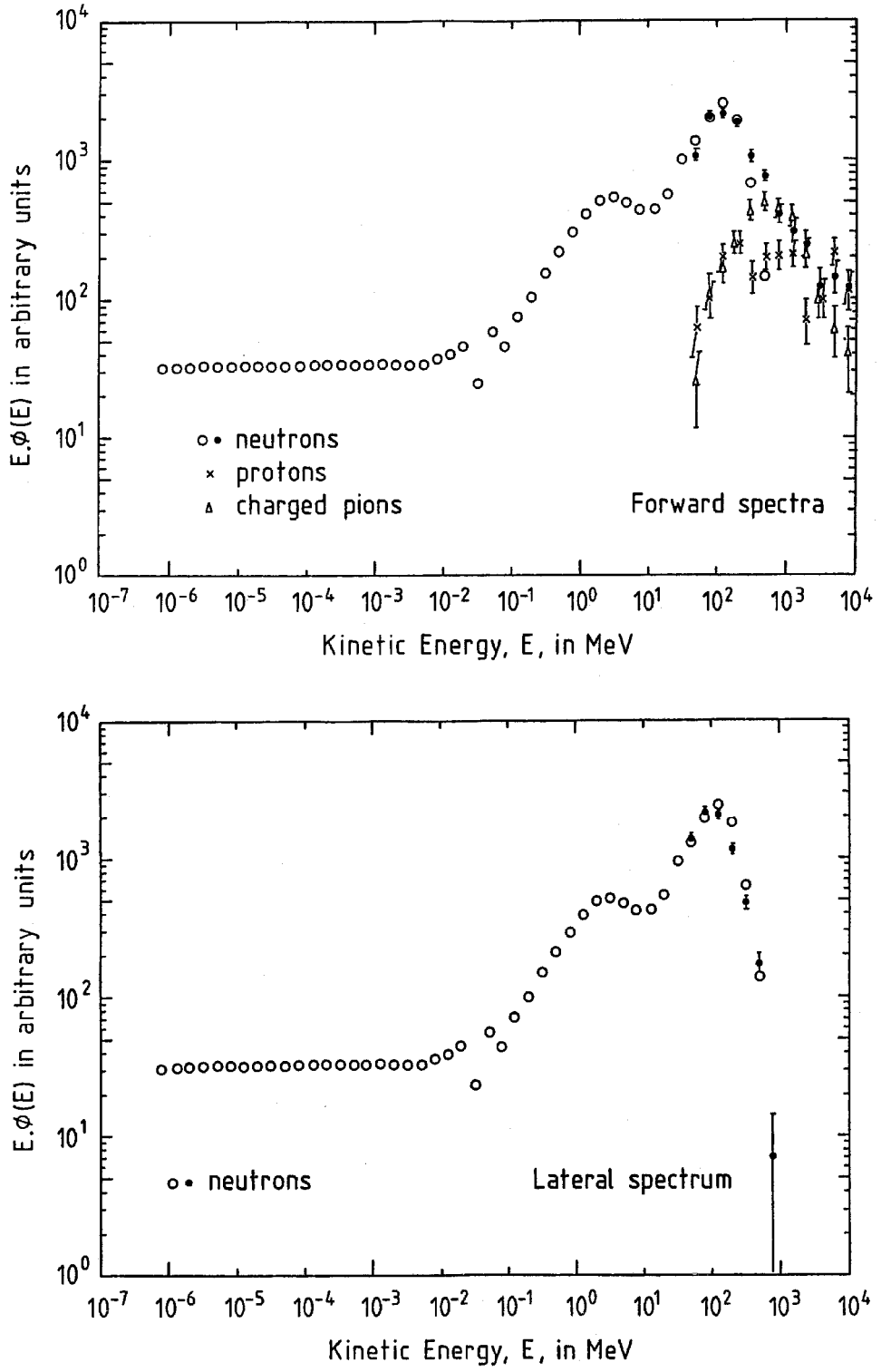

Fig. 6.4 Neutron energy spectra outside of a concrete shield at a high energy proton accelerator at forward angles (**upper frame**) and at large angles (**lower frame**). The open circles represent the calculations of O'Brien (OB71) while the other symbols represent the calculations of Höfert and Stevenson. [Adapted from (Hö84a).]

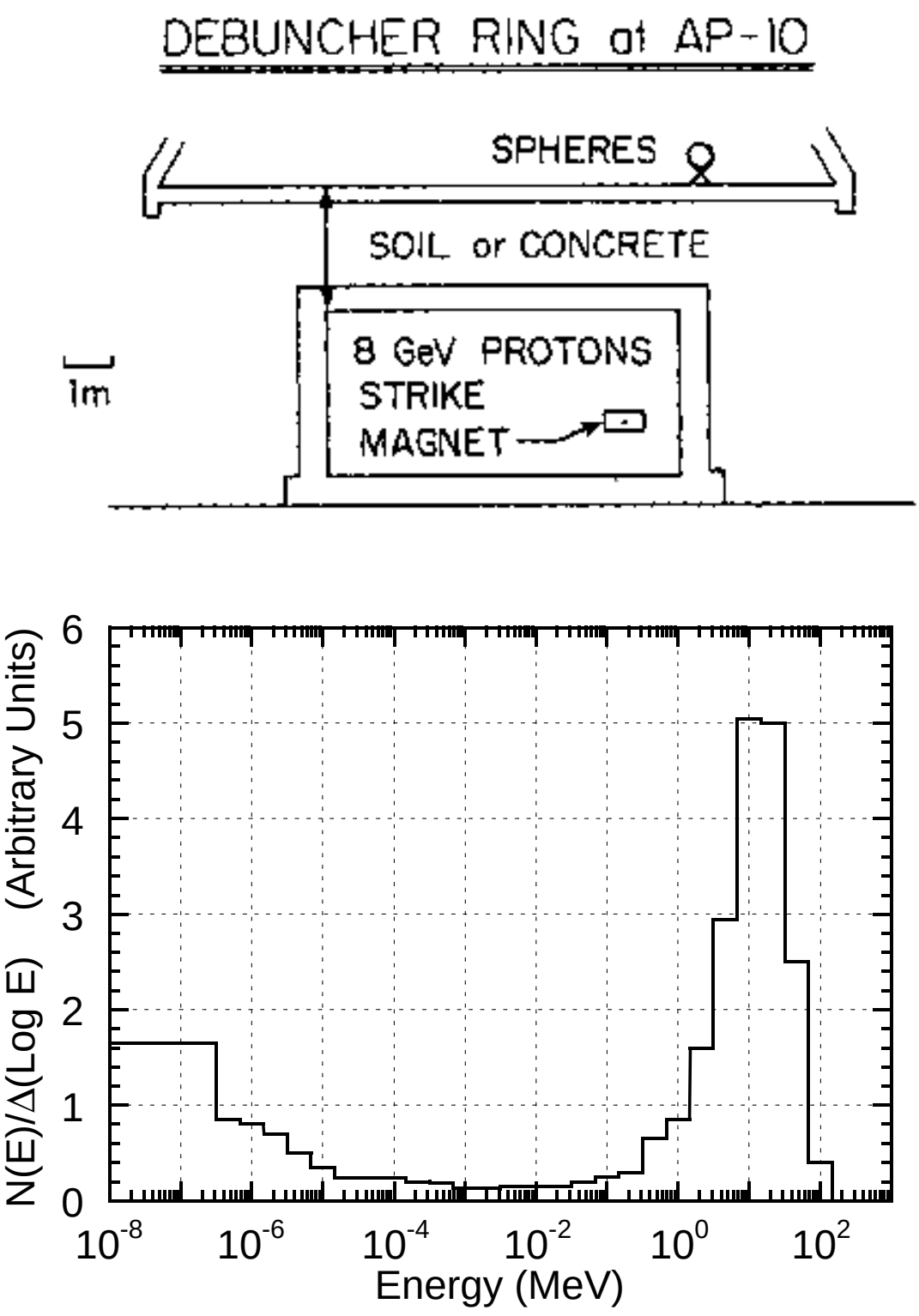

Fig. 6.5 Neutron energy spectra obtained external to a beam enclosure in which 8 GeV protons struck the yoke of a magnet. The site was the Fermilab Debuncher Ring. The normalization of the spectrum is arbitrary. [Adapted from (Co88).]

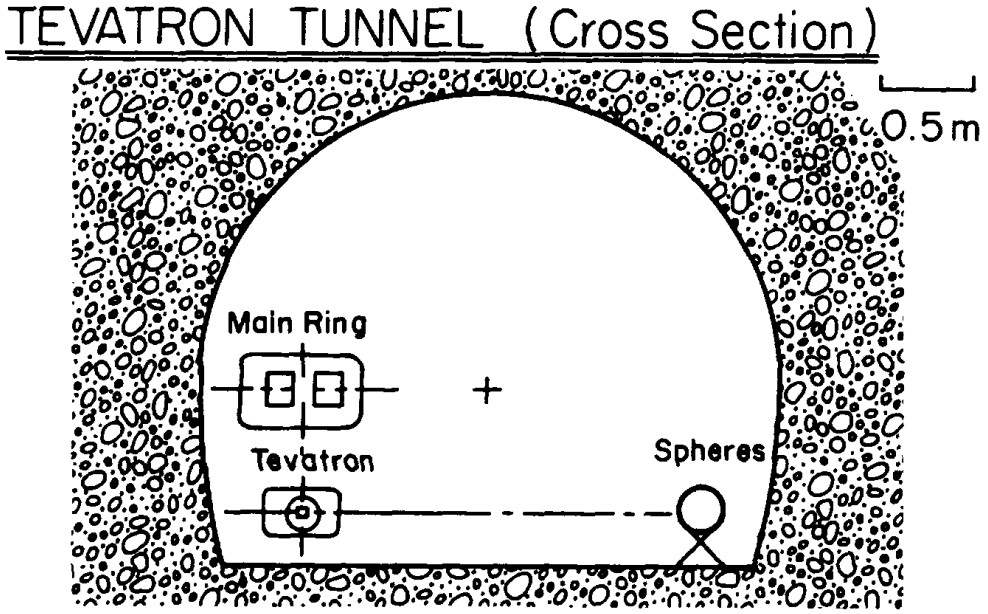

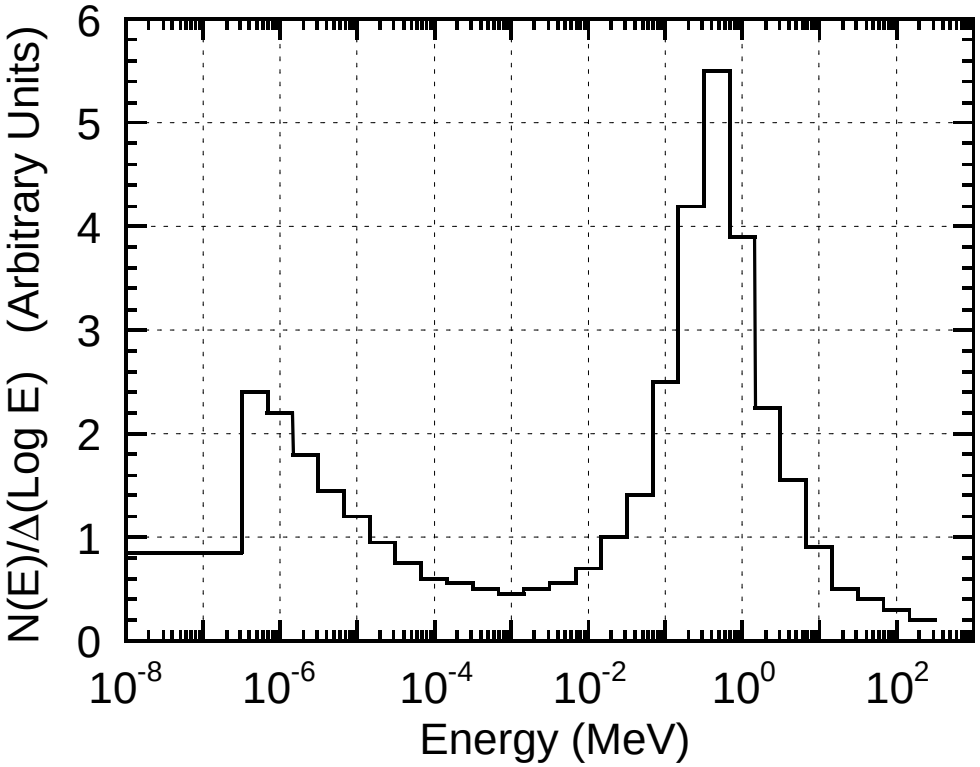

Fig. 6.6 Neutron energy spectra obtained internally in a beam enclosure in which 800 GeV protons interacted with residual gas in the Tevatron vacuum chamber during circulating beam conditions. The site was the Fermilab Tevatron Ring. The normalization of the spectrum is arbitrary. [Adapted from (McC88).]

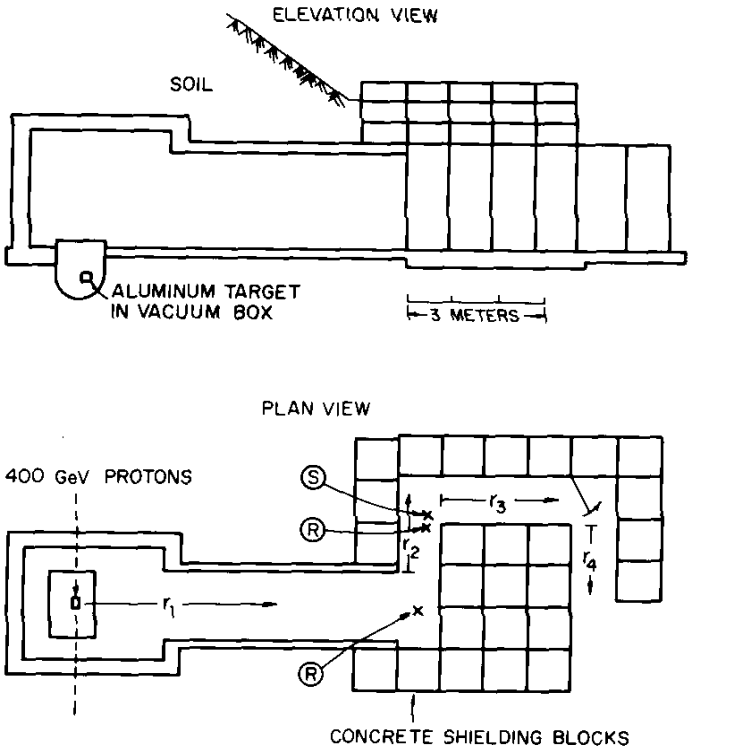

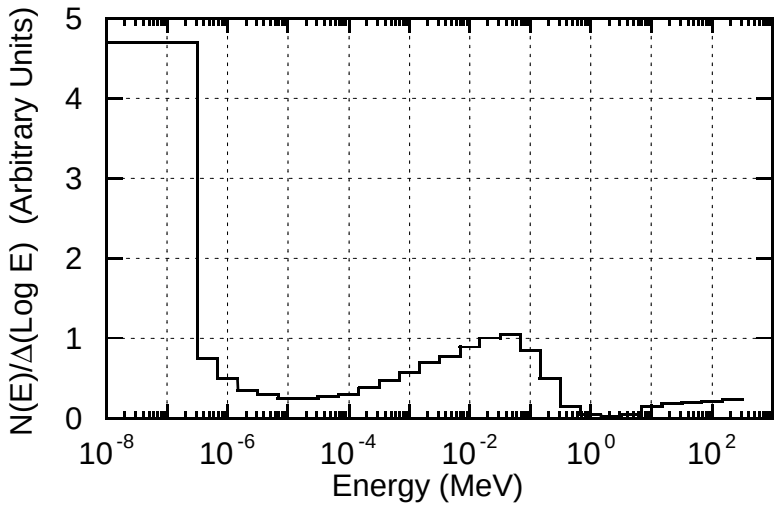

Fig. 6.7 Neutron energy spectra obtained within a labyrinth enclosure in which 400 GeV protons interacted with an aluminum target located beneath the floor of the enclosure shown. The spectrum was measured in the second leg at the location denoted "**S**". A quality factor measurement was made at the location denoted "**R**" (see Section 9.5.7). The normalization is arbitrary. [Adapted from (Co88).]

6.3.5 Leakage of Low Energy Neutrons Through Iron Shielding

One of the peaks that commonly appear in such spectra is particularly important. As discovered by Alsmiller and Barish (Al73) and mentioned in Section 6.2.4, iron has a major deficiency as a shield for fast neutrons. The primary attenuation mechanism for fast neutrons is by inelastic scattering from the iron nuclei. At energies below the first excited state of any nucleus, inelastic scattering becomes impossible and elastic scattering becomes the only removal process. Elastic scattering is a very inefficient mechanism for energy removal for neutrons scattering off the much more massive iron nucleus as is evident from Eq. (6.1). The scattering of billiard balls off of bowling balls comes to mind as an analogy. It is intuitive that billiard balls scattering off other billiard balls of equal mass provides for much more efficient energy transfer. Likewise, neutrons scattered by the "free" protons in hydrogenous materials is much more efficient in terms of energy transfer than is the elastic scattering of neutrons from iron nuclei. The first excited state of ^{56}Fe, which is the dominant isotope in natural iron (92% abundance), is at 847 keV. This has the consequence that the neutrons build up below this energy due to the inefficiency of the transfer of energy by means of elastic scattering. Thus neutrons above 847 keV in a given spectrum will be slowed by inelastic scattering only to build up in this region. Amplifying this effect when one considers the dose equivalent external to such shields is the fact that the quality factor for neutrons as a function of energy also has its maximum value at about 500 keV (see Fig. 1.3). Thus, pure iron shields are rather ineffective in attenuating neutrons in this energy region.

This phenomena is illustrated by the geometry and spectra shown in Fig. 6.8, supporting the calculations provided in Fig. 6.1. Both spectra in Fig. 6.8 shown were measured at about $\theta = 90^{o}$ from a beam dump struck by secondary particles due to 800 GeV proton interactions far upstream of the beam dump (El86). The beam dump was shielded by the yoke of a large iron magnet as shown in Fig. 6.8a. Originally, the neutron energy spectra was measured directly adjacent to this iron shield. This spectrum is identified as Fig. 6.8b. Later, in order to reduce the intensity of the neutron radiation, concrete shielding blocks 91.4 cm thick were placed between the neutron detectors and the beam absorber up to a height above the beam line. The neutron energy spectrum was measured again with the result displayed in Fig. 6.8c. For the bare iron situation the normalized dose equivalent rate external to the shield was over 40 times that measured after the concrete was installed. This factor is far in excess of the approximate factor of 10 expected from simple attenuation of the equilibrium cascade neutron spectrum and indicates both the importance of the leakage neutrons and the maximization of their quality factor. The inclusion of the concrete also reduced the average quality factor from 5.4 to 2.8.

In general, an iron shield "capped" or "backed" by such a concrete shield will be an efficient use of space. It has been determined that 60 cm of concrete is the most efficient thickness to use for this purpose [(Yu83) and (Za87)]. Shielding properties of other elements near iron (chiefly copper and nickel) in the periodic table are comparable.

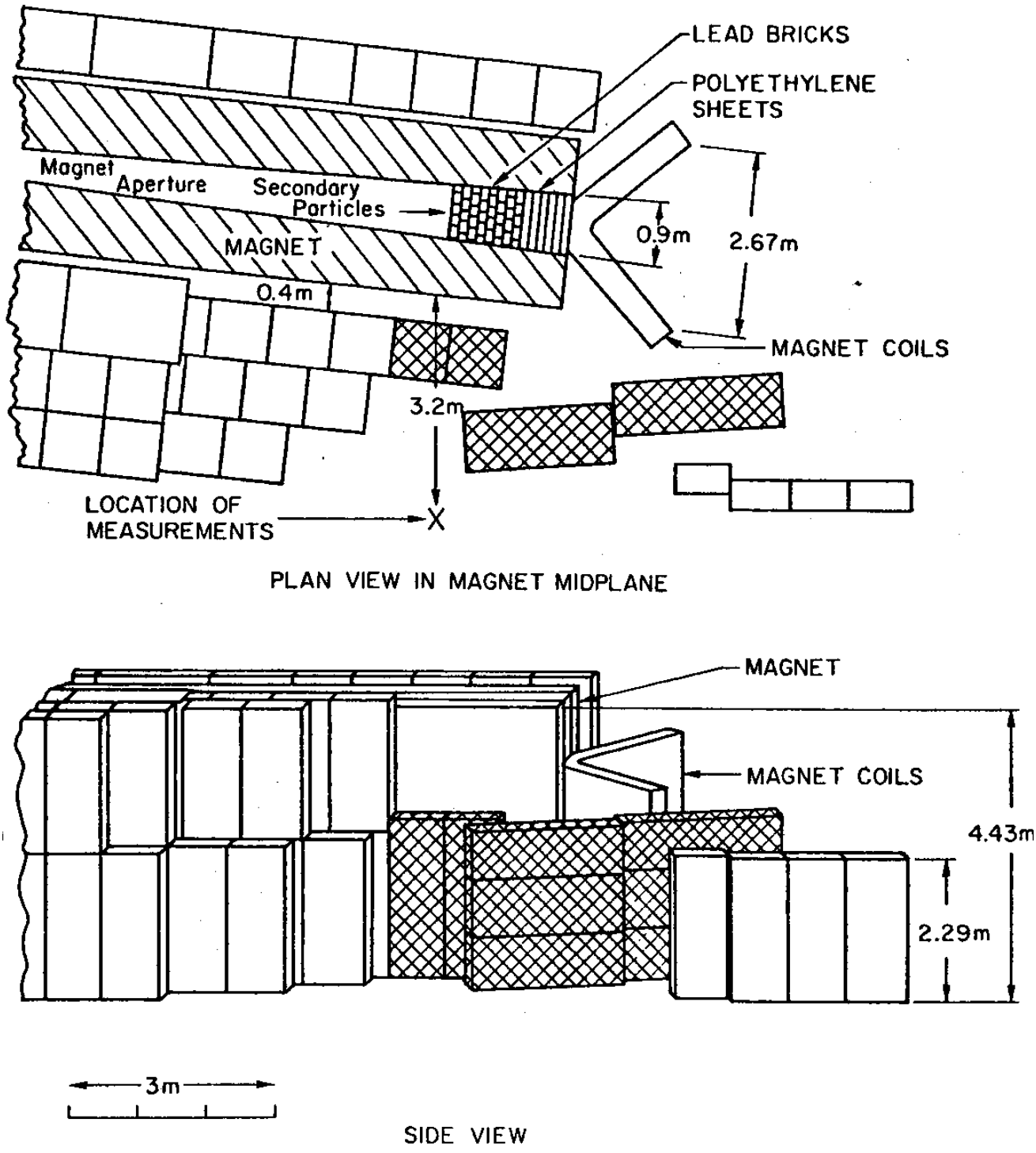

Fig. 6.8a Situation for the measurements shown in Figs. 6.8b and 6.8c. A target upstream (to the left) of the apparatus shown in the figure was struck by 800 GeV protons. Secondary particles produced by these interactions were intercepted by the beam absorber shown in the Figure. The plain shielding blocks are of ordinary concrete. During initial operations, the cross-hatched blocks, also of ordinary concrete, were not in place between this beam absorber and the location of measurements and the result was the measured spectrum in Fig. 6.8b. Later, those blocks were added and the spectrum shown in Fig. 6.8c was measured. [Reproduced from (El86).]

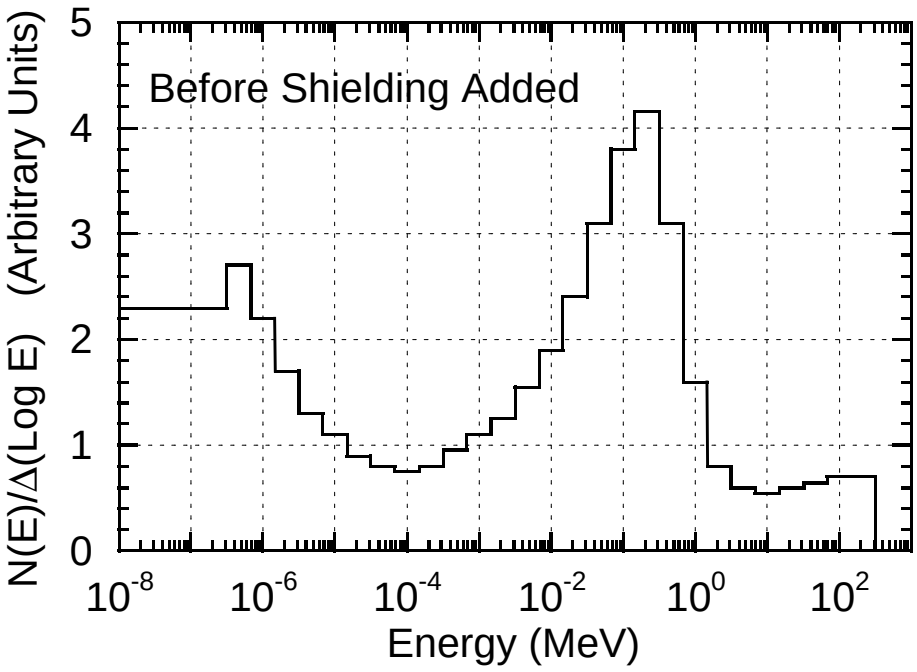

b)

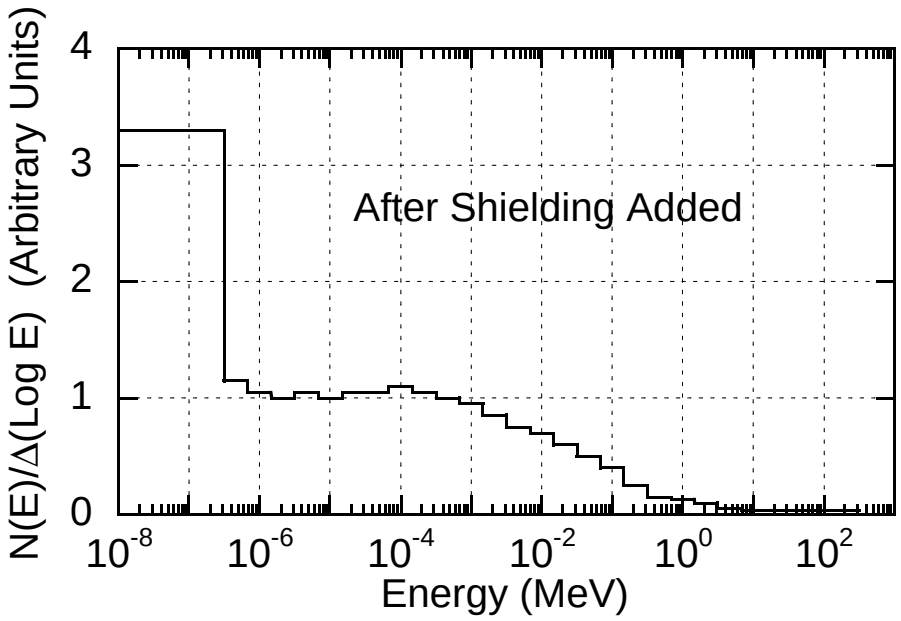

c)

Fig. 6.8 b&c Neutron energy spectra obtained external to the shielding configuration shown in Fig. 6.8a for the two different situations discussed above. The normalization of the spectrum is arbitrary. [Adapted from (El86).]

6.3.6 Neutron Spectra Due to Ions

Neutron energy spectra behind shielding obtained with ions are quite rare. Britvich et al. (Br99) have provided such spectra for ^{12}C ions incident on a Hevimet target at 155 MeV nucleon^{-1}. The spectrum of neutrons due to ^{12}C ions was measured at $\theta = 94^o$ without shielding at a distance of 121 cm from the target. The result is shown in Fig. 6.9. Qualitatively similar spectra were obtained at this location with ^{4}He and ^{16}O ions at with 155 MeV nucleon^{-1}. The spectrum due to the ^{12}C ions was measured at $\theta = 94^o$ at a distance of 403 cm from the target which was shielded by 308 g cm^{-2} of ordinary concrete. The result is shown in Fig. 6.10. One can see that the shielding effectively attenuates many of the neutrons below about 0.3 MeV.

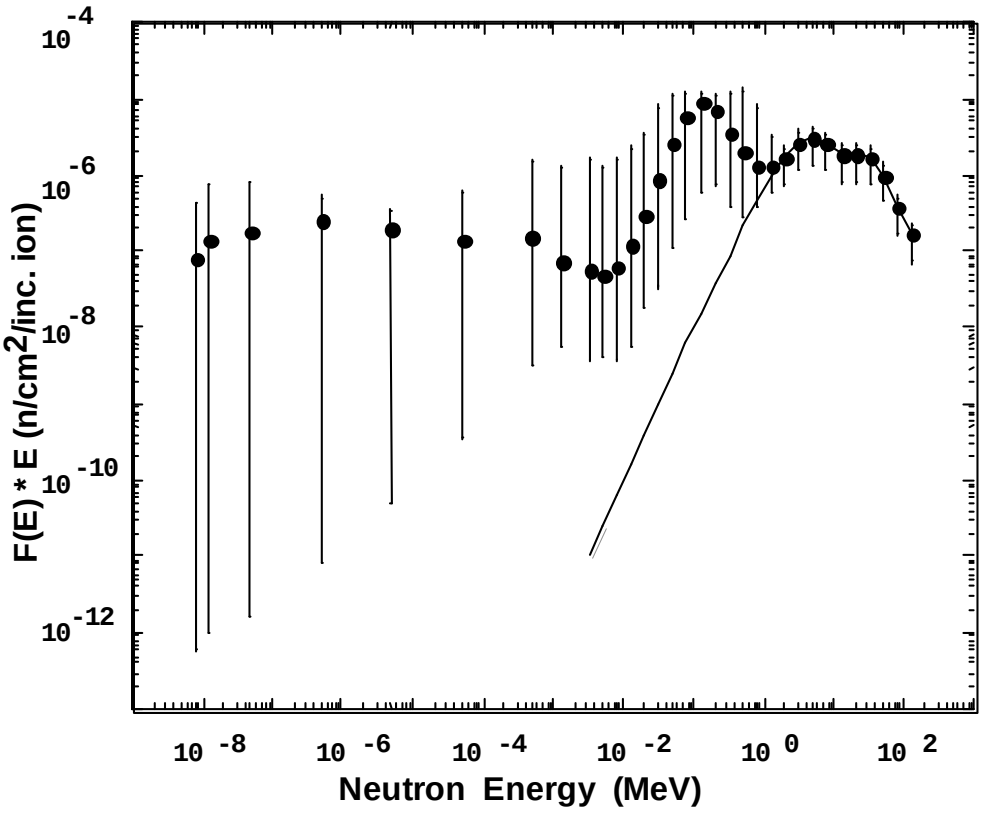

Fig. 6.9 Neutron energy spectrum *F(E)* x *E* at 121 cm and $\theta = 94^o$ from a thick Hevimet target bombarded by 155 MeV/nucleon ^{12}C ions where *F* denotes the normalized neutron fluence. The solid line is a fit to these data using a parameterization suggested by Nakamura (Na85). [Reproduced from (Br99).]

Intuitively, especially for ions of high atomic number, one might expect more copious production of neutrons. This matter was studied in measurements conducted by Aroura et al. (Ar97) for lead ions having a specific energy of 160 GeV nucleon^{-1}. Comparisons of neutron energy spectra on top of a concrete shield surrounding a lead target were made with those obtained with 205 GeV protons and with π^+'s. The results are given in Fig. 6.11.

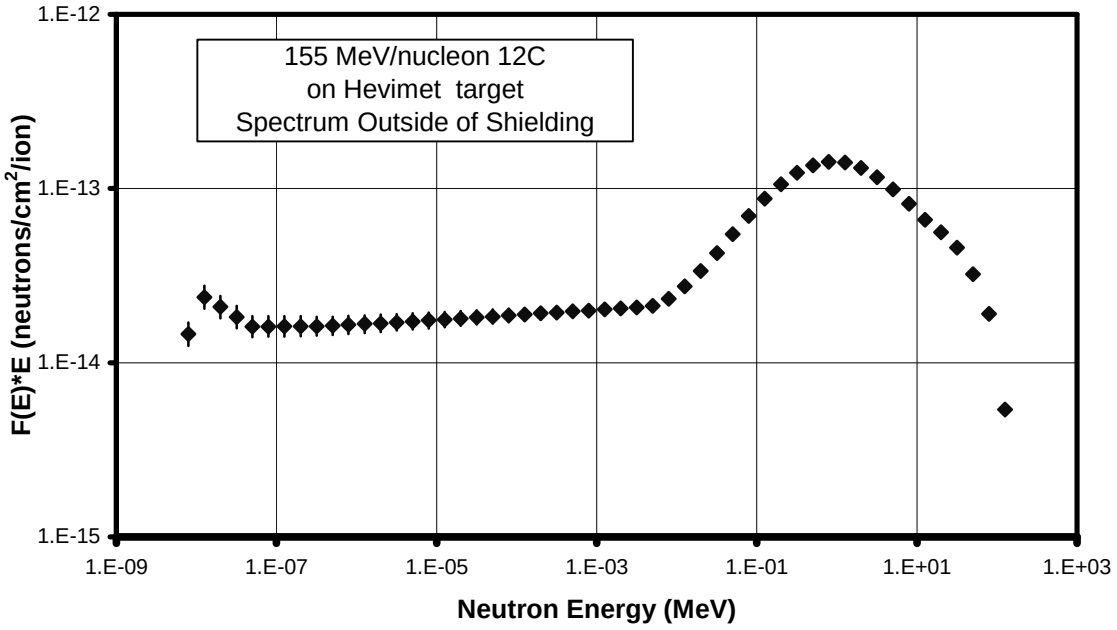

Fig. 6.10 Neutron energy spectrum *F(E)* x *E* at 403 cm and θ = 94°, and behind 128.3 cm of concrete shielding, from a thick Hevimet target bombarded by 155 MeV/nucleon ^{12}C ions [Reproduced from (Br99)].

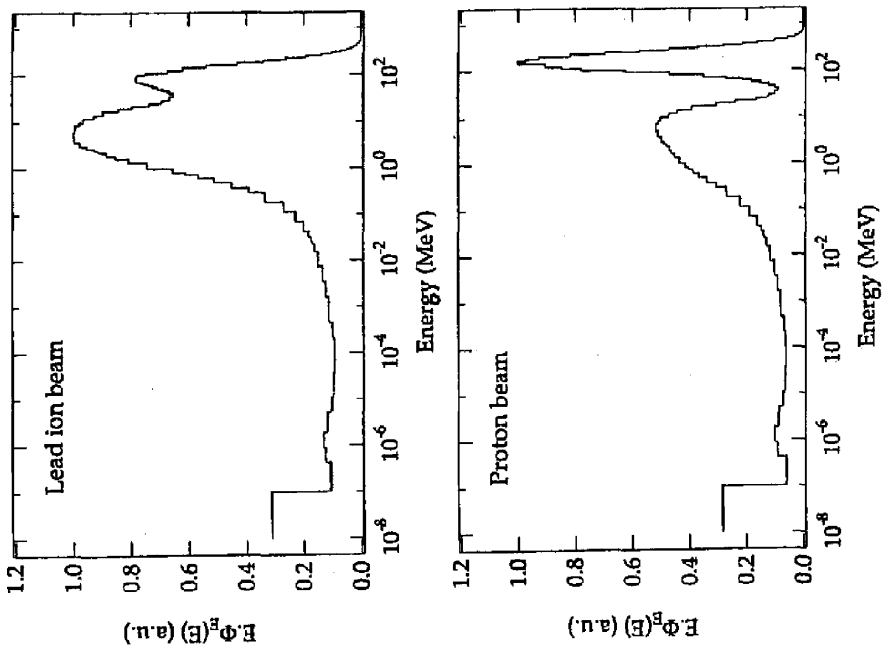

Fig. 6.11 Neutron fluence spectra around a lead ion beam of 160 GeV/nucleon shielded by concrete compared with that obtained with of a 205 GeV proton beam. The units used for the ordinate are arbitrary. For further discussion, consult the original reference of Aroua et al. [Reproduced from (Ar97).]

6.3.7 Neutron Fluence and Dosimetry

As was seen with electrons in Section 6.3.1, one must be concerned with the relative amounts of fluence and dose equivalent due to specific spectral regions. This can affect the potential to produce radioactivity and also guides the designer of shielding. Tables 6.4 and 6.5 give these properties for the spectra displayed in Figs. 6.5, 6.6, 6.7, and 6.8. Fig. 6.12 is a plot of cumulative values of the same quantities for 1000 GeV protons incident on the face of a thick cylindrical concrete shield. As determined by Van Ginneken and Awschalom (Va75), the dependence upon incident proton energy of the distributions of fluence and dose equivalent is slight.

Table 6.4 Percent fluence in specific energy bins for neutron energy spectra. [Adapted from (Co88).]

Energy Range	Fig. 6.5	Fig. 6.6	Fig. 6.7	Fig. 6.8b	Fig. 6.8c
< 1.5 eV	31.5	19.5	71	28	55
0.0015 - 100 keV	12.5	36	24	46	43
0.1 - 2 MeV	8.5	36	2	17.5	2
2 - 25 MeV	40.5	7	1	4.5	0.1
> 25 MeV	7	1.5	1.5	4	0

Table 6.5 Percent of dose equivalent in specific energy bins for neutron energy spectra along with average quality factor. [Adapted from (Co88).]

Energy Range	Fig. 6.5	Fig. 6.6	Fig. 6.7	Fig. 6.8b	Fig. 6.8c
< 1.5 eV	1.5	2	32	4	41.5
0.0015 - 100 keV	0.5	6	16	11.5	37
0.1 - 2 MeV	9	58.5	9	35	17
2 - 25 MeV	75	26	13	24	3.5
> 25 MeV	14	7.5	30	25	1
Average Quality Factor	5.8	6.9	3.1	5.4	2.5

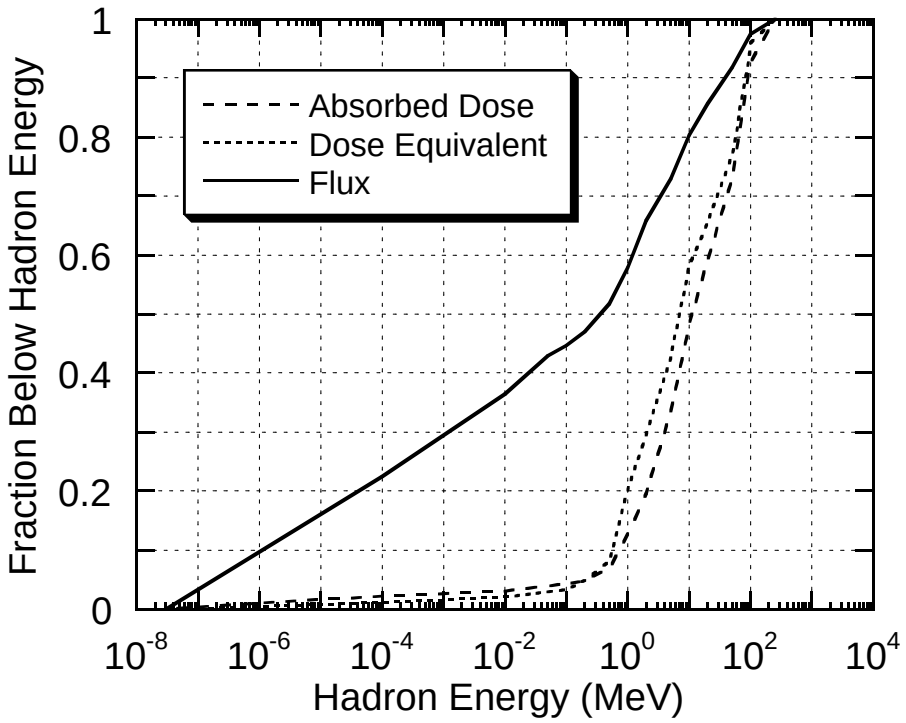

Fig. 6.12 Fraction of the omnidirectional flux, entrance absorbed dose, and maximum dose equivalent below hadron kinetic energy on abscissa (in MeV) for the region between zero and 450 cm depth and between 300 cm and 750 cm radius for 1000 GeV/c protons incident on the face of a solid concrete cylinder. [Adapted from (Va75).]